Time-shift extended imaging for estimating depth errors

Mulder, W.

DOI
10.3997/2214-4609.202310690

Publication date
2023

Document Version
Final published version

Citation (APA)
Mulder, W. (2023). *Time-shift extended imaging for estimating depth errors*. Paper presented at 84th EAGE ANNUAL Conference and Exhibition 2023, Vienna, Austria. https://doi.org/10.3997/2214-4609.202310690

2023 EAGE ANNUAL
84TH CONFERENCE & EXHIBITION
VIENNA | AUSTRIA

Time-shift extended imaging for estimating depth errors

W. Mulder[1,2]

[1] Shell Global Solutions International BV; [2] Delft University of Technology

Summary

The stationary-phase method applied to migration with a time-shift extension in a 2-D constant-velocity model with a dipped reflector produces two solutions in the domain of the extended image: one a straight line and the other a curve. If the velocity differs from the true one, the depth error follows from the depth and apparent dip of the reflector as well as the depth of the amplitude peak at a non-zero time shift, where the two solutions meet and the extended image focuses. The results are compared to finite-frequency results from a finite-difference code. A 2-D synthetic example with a salt diapir illustrates how depth errors can be estimated in an inhomogeneous model after inverting the seismic data for the velocity model.

Time-shift extended imaging for estimating depth errors

Introduction

Among the several methods for velocity model building, migration velocity analysis (MVA) with extended images based on subsurface offsets or time shifts exploits the move-out information in the data, unlike full-waveform inversion (FWI) in its original form without emphasis on phase. A disadvantage of MVA is the pre-processing required to extract the primaries from the data, because the result is highly sensitive to the presence of multiples (Mulder and van Leeuwen, 2008; Weibull and Arntsen, 2013).

Here, the stationary-phase method is applied to migration with a time-shift extension (Faye and Jeannot, 1986; MacKay and Abma, 1992; Sava and Fomel, 2006; Higginbotham et al., 2008), to find the depth error for a dipped interface in a 2-D constant-velocity model. The result is used to estimate the depth errors of a partially converged velocity model obtained for 2-D synthetic Born data for a salt diapir model, using a focusing method (Mulder, 2008, 2014) with time shifts instead of subsurface offsets.

Stationary-phase method for a constant velocity

Consider an interface with dip angle α_0 in a 2-D homogeneous model with constant velocity v_0. The interface is defined by a depth $z(x) = z_a + (x - x_a)\tan\alpha_0$ for a reference point (x_a, z_a). The source is located at (x_s, z_s) and the receiver at (x_r, z_r), with $z_s = z_r = 0$ at the surface. The half-offset is $h = (x_r - x_s)/2$ and the midpoint $x_m = (x_r + x_s)/2$. Assume $h \geq 0$ and $|\alpha_0| < \pi/2$. The travel time to a subsurface point (x, z) is $\tau = \tau_s + \tau_r$, with $\tau_{s,r} = v_0^{-1}\sqrt{z^2 + (x - x_{s,r})^2}$. The reflection point on the dipped interface in the high-frequency limit can be found by requiring $\partial\tau/\partial x = 0$, using $z(x)$ on the interface. For the derivation, it may be more convenient to replace x by z, assuming non-zero dip, $\alpha_0 \neq 0$, and positive depth, $z > 0$. The solution for the scatter point (x, z) is represented by $x - x_m = -\sin(\alpha_0)\cos(\alpha_0)(z_m^2 + h^2)/z_m$ and $z - z_m = (x - x_m)\tan\alpha_0$, where the midpoint x_m is related to z_m by $z_m = z_a + (x_m - x_a)\tan\alpha_0$. The two-way travel time becomes $\tau = 2v_0^{-1}\sqrt{h^2 + z_m^2}\cos\alpha_0$ if $z_m > h\tan|\alpha_0|$, that is, if the interface does not cut the surface between source and receiver. Geometrical arguments and Snell's law produce the same result.

The extended migration image in a model with velocity v of data obtained with velocity v_0 and an additional time shift Δt is given by

$$r(x, z; \Delta t) = \int_{h_{\min}}^{h_{\max}} \mathrm{d}h \int_{-\infty}^{\infty} \mathrm{d}x_m \; A(x_s, z_s; x, z) A(x_r, z_r; x, z) e^{\mathrm{i}\omega\psi}, \tag{1}$$

where the phase $\psi = \tau(h, x_m; v_0) - \tau_s(x, z; v) - \tau_r(x, z; v) - 2\Delta t$. The amplitudes $A(x_{s,r}, z_{s,r}; x, z)$ from source or receiver to depth point (x, z) are not important in what follows. For now, an infinite offset range is assumed, with $h_{\min} \to -\infty$ and $h_{\max} \to \infty$. Stationarity involves the equations $\psi = 0$, $\partial\psi/\partial h = 0$ and $\partial\psi/\partial x_m = 0$ for Δt, h and x_m. The first equation directly provides the stationary Δt. The remaining two have two solutions. The first solution is given by $h = 0$, $x_m = x + z\tan\alpha$ with apparent dip angle α, where $\sin\alpha = \beta\sin\alpha_0$ and $\beta = v/v_0$, requiring $\beta|\sin\alpha_0| < 1$. If $z_0 = z_a + (x_0 - x_a)\tan\alpha_0$ is the true depth at a given $x = x_0$, the stationary time shift $\Delta t(z) = v^{-1}(z_0\beta\cos\alpha_0 - z\cos\alpha) = v^{-1}(z_{\mathrm{mig}} - z)\cos\alpha$, where the depth at zero time shift is $z_{\mathrm{mig}} = z_0\beta\cos\alpha_0/\cos\alpha = z_0\tan\alpha/\tan\alpha_0$ for an apparent interface $z(x) = (x - x_a + z_a/\tan\alpha_0)\tan\alpha = z_{\mathrm{mig}} + (x - x_0)\tan\alpha_0$. In the correct model, $\beta = v/v_0 = 1$, $\alpha = \alpha_0$, and the stationary $\Delta t = 0$.

The amplitude along the straight line $\Delta t(z)$ at fixed x and $h = 0$ is inverse proportional to the square root of the absolute value of the determinant of the Hessian w.r.t. h and x_m. This absolute value is given by

$$\frac{4\cos^3\alpha}{v^2 z^2 z_m}\left|z_m\cos^3\alpha - z\beta\cos\alpha_0\right|. \tag{2}$$

Substitution of $z_m = z_0 + (x_m - x_0)\tan\alpha_0$, $x_m = x + z\tan\alpha$ and $z_0 = z_{\mathrm{mig}}\tan\alpha_0/\tan\alpha$ from above results in an equation for z for which the determinant in equation (2) is zero and the amplitude infinite, at $z = z_{\mathrm{peak}} = z_{\mathrm{mig}}/[\{1/(\tan\alpha_0\cos\alpha)^2 - 1\}\tan^2\alpha]$. At finite frequencies, the amplitude will become finite. In the correct model with $\beta = 1$, $z_{\mathrm{peak}} = z_0$ and $\Delta t_{\mathrm{peak}} = 0$.

The second solution of the stationary phase equations with $h \neq 0$ could not be obtained in closed form and will be computed numerically. A series expansion in h shows that it starts at $z = z_{\text{peak}}$, on the line of the first solution with $h = 0$. When h increases, it moves away from the line, with decreasing $z \leq z_{\text{peak}}$ if $\beta > 1$, or increasing $z \geq z_{\text{peak}}$ if $\beta < 1$.

For zero dip angle $\alpha_0 = 0$, the first solution becomes $\Delta t = v^{-1}(\beta z_0 - z)$. The second has $x_m = x$, $h = [(z_0^2 - \beta^2 z^2)/(\beta^2 - 1)]^{1/2}$ and $\Delta t = v^{-1}(\beta^2 - 1)[(z_0^2 - z^2)/(\beta^2 - 1)]^{1/2}$ (Sava and Fomel, 2006). In addition, $z_{\text{peak}} = z_0/\beta$ and $z_{\text{mig}} = z_0\beta$, implying $z_0 = (z_{\text{mig}} z_{\text{peak}})^{1/2}$ (Faye and Jeannot, 1986).

With a finite acquisition, the endpoint in stationary phase integral has to be included. Given a maximum half-offset h_{max} and a Δt following from $\psi = 0$, this leaves the equation $\partial\psi/\partial x_m = 0$. Solving this numerically for x_m leads to Δt as a function of z at fixed x. In the absence of a proper acquisition taper, the solution at zero time shift shows up as an additional apparent interface in the migration image. For certain interface and acquisition parameters, not considered here, there may be more than one solution.

The apparent dip angle at $h = 0$ and $\Delta t = 0$ can be estimated from $\partial z/\partial \Delta t = -v/\cos\alpha$ or $\partial z/\partial x = \tan\alpha$, where the second expression avoids a sign ambiguity. With that and the migration depth z_{mig} at zero time shift, z_{peak} can be located along the line $\Delta t = v^{-1}(z_{\text{mig}} - z)\cos\alpha$. The depth error follows from

$$z_{\text{mig}} - z_0 = z_{\text{mig}}\left(1 - \frac{\tan\alpha_0}{\tan\alpha}\right), \quad \frac{\tan\alpha_0}{\tan\alpha} = \left[1 + (z_{\text{mig}}/z_{\text{peak}} - 1)\cos^2\alpha\right]^{-1/2}. \tag{3}$$

For small dip, $z_{\text{mig}} - z_0 \simeq z_{\text{mig}}(1 - \sqrt{z_{\text{peak}}/z_{\text{mig}}})$ (Faye and Jeannot, 1986).

If the velocity is not constant, the straight-line solution becomes curved (Duveneck, 2021). To estimate z_{peak} at a given x and $z = z_{\text{mig}}$, determine the apparent dip angle α, rotate the extended image by $\arctan(-v(x,z)/\cos\alpha)$, track along the nearly horizontal event to find the peak amplitude and its position, and then rotate back to find z_{peak}.

Comparison to finite-frequency results

To illustrate the result, Born scattering data were generated with a finite-difference code for a velocity model with $v_0 = 1500$ m/s and two reflectors. The first had a depth of 400 m at $x = 0$ m and 700 m at $x = 3000$ m, the second a depth of 1200 m at $x = 0$ m and 1000 m at $x = 3000$ m, resulting in dip angles of 5.71 and −3.81 degrees. Shots at zero depth ranged from $x_s = 0$ to 3000 m with a 50-m spacing and a 15-Hz Ricker wavelet. Receivers had offsets $x_r - x_s$ from 100 to 2000 m at a 25-m interval in a marine-type acquisition.

Figure 1(a) shows the extended image in the correct velocity model, obtained with the same 2-D frequency-domain finite-difference code. Figure 1(b) corresponds to a velocity that is 10% smaller and Figures 1(c) and 1(d) for 10% larger. In the finite-frequency case, the peak value along the straight-line solution does not occur at the predicted location. This is mainly caused by the interference with the curved second solution that starts at the predicted peak location and, to a lesser extent, with the curve for the maximum offset. The net effect will be an over-estimate of the depth error.

An application

To examine the potential use of the derived depth-error estimate, the 2-D velocity model of Figure 2(a), taken from (Mulder, 2001), was considered. Born scattering data for the reflectivity shown in Figure 2(b) were generated for a land-type acquisition with shots between −950 and 6950 m at a 50-m interval with a 15-Hz Ricker wavelet and receivers between −962.5 and 6962.5 m at a 25-m interval.

Figure 2(d) displays a reconstructed velocity model represented by cubic B-splines and obtained by optimizing a focusing functional based on time-shift extended imaging, similar to (Mulder, 2008, 2014) but with subsurface shifts replaced by time shifts. Note that this method does not explicitly include depth errors but only tries to move energy in the image to zero shift. The shown model corresponds to an intermediate result, starting from the best linear-in-depth velocity with given surface velocity. Figure 2(e) shows the corresponding depth-weighted migration image. The data were differentiated in time to change

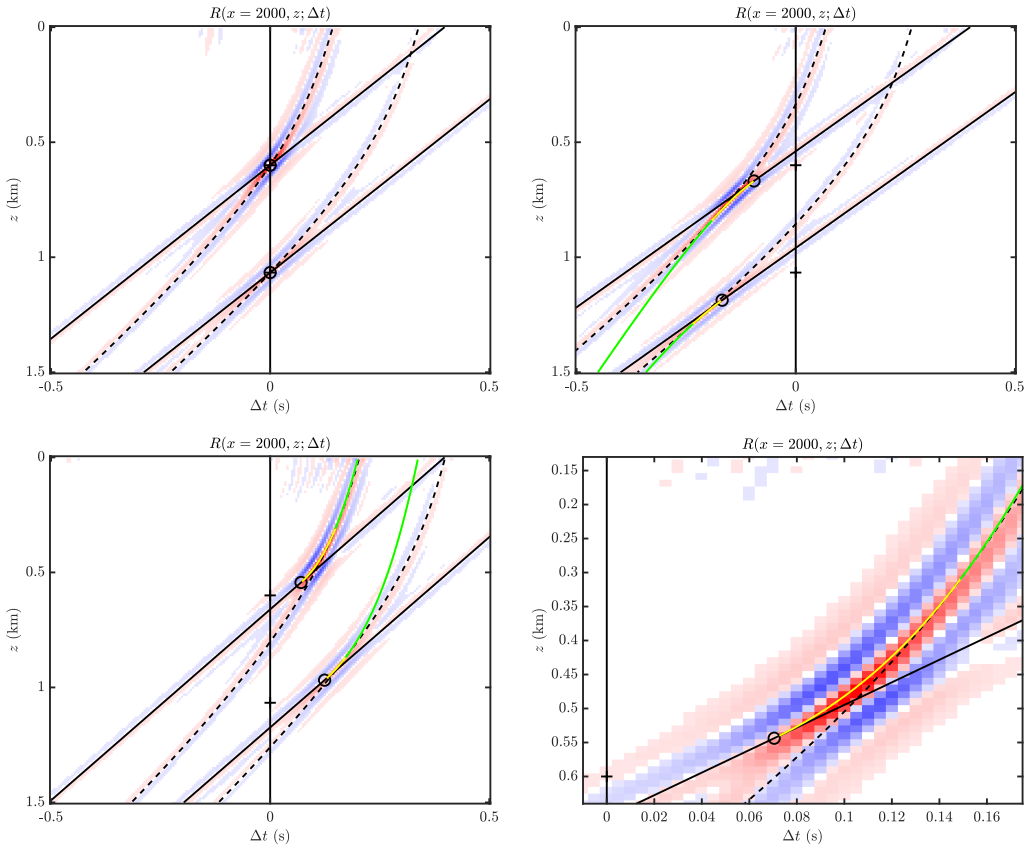

Figure 1 *(a) Extended image at fixed $x = 2000\,m$ and a function of time shift Δt and depth z for the true velocity. The drawn line represents the first solution of the stationary phase equations and the circle denotes the expected position of the maximum amplitude. The dashed lines correspond to the maximum offset. (b) As (a) but for too low a velocity of $1350\,m/s$. The drawn yellow curves represent the second solution, with the green part corresponding to offsets larger than the maximum offset in the data. The true depth of the reflector is marked by a small horizontal line segment at zero time shift. (c) As (a) but for too high a velocity of $1650\,m/s$. (d) Detail of (c).*

the zero-crossing of the reflectivity in Figure 2(b) at the position of an interface into a peak in Figure 2(e) (Østmo et al., 2002). Figure 2(c) displays the depth errors, expected to be over-estimated. The impact of the salt diapir is obvious, as is the increase in error with depth. For comparison, Figure 2(f) shows a crude estimate of the depth error obtained from $\int_0^z \mathrm{d}z'[1 - v(x,z')/v_0(x,z')]$, which ignores strong lateral variations. This shows that, although the focusing of energy in an extended image can be fairly effective for the construction of an initial velocity model from primaries-only data, this appears to be less so for the more delicate depth-error estimation outlined here, at least for its present implementation, although the overall trend is more or less correct.

Conclusions

The stationary-phase method applied to migration with a time-shift extension in a 2-D constant-velocity model with a dipped reflector produces two solutions, one a straight line and the other a curve, similar to the case of a horizontal reflector (Sava and Fomel, 2006). The depth error follows from the apparent reflector dip and depth as well as the depth of the amplitude peak along the first solution in the time-shift extended image, where the second solution meets. The method was applied to estimate the depth errors in a 2-D example with a salt diapir.

Acknowledgements

The author is indebted to Eric Duveneck and Boris Kuvshinov for their helpful comments.

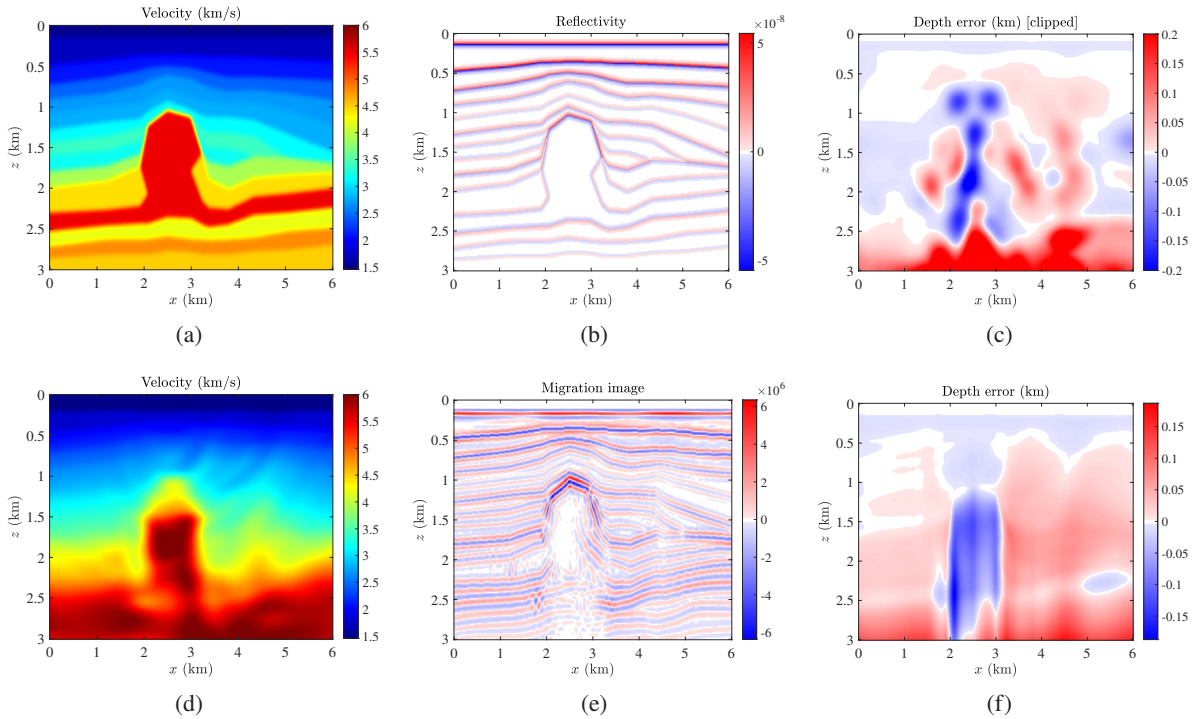

Figure 2 *Velocity model (a) and reflectivity (b) for the true model and the estimated error (c), clipped at ±200 m, for the recovered model (d), the related depth-weighted migration image (e), and a crude estimate of the depth error obtained by comparing the recovered and exact velocity model (f).*

References

Duveneck, E. [2021] Angle gathers from time-shift extended least-squares reverse-time migration. In: *Conference Proceedings, 82nd EAGE Annual Conference & Exhibition*. European Association of Geoscientists & Engineers, 1–5.

Faye, J.P. and Jeannot, J.P. [1986] Prestack migration velocities from focusing depth analysis. In: *SEG Technical Program Expanded Abstracts 1986*. Society of Exploration Geophysicists, 438–440.

Higginbotham, J.H., Brown, M.P. and Clapp, R.G. [2008] Wave equation migration velocity focusing analysis. In: *SEG Technical Program Expanded Abstracts 2008*. Society of Exploration Geophysicists, 3083–3087.

MacKay, S. and Abma, R. [1992] Imaging and velocity estimation with depth-focusing analysis. *Geophysics*, **57**(12), 1608–1622.

Mulder, W.A. [2001] Higher-order mass-lumped finite elements for the wave equation. *Journal of Computational Acoustics*, **9**(2), 671–680.

Mulder, W.A. [2008] Automatic velocity analysis with the two-way wave equation. In: *Conference Proceedings, 70th EAGE Conference and Exhibition incorporating SPE EUROPEC 2008*. European Association of Geoscientists & Engineers, 1–5.

Mulder, W.A. [2014] Subsurface offset behaviour in velocity analysis with extended reflectivity images. *Geophysical Prospecting*, **62**(1), 17–33.

Mulder, W.A. and van Leeuwen, T. [2008] Automatic migration velocity analysis and multiples. In: *SEG Technical Program Expanded Abstracts 2008*. Society of Exploration Geophysicists, 3128–3132.

Østmo, S., Mulder, W.A. and Plessix, R. [2002] Finite-difference iterative migration by linearized waveform inversion in the frequency domain. In: *SEG Technical Program Expanded Abstracts 2002*. Society of Exploration Geophysicists, 1384–1387.

Sava, P. and Fomel, S. [2006] Time-shift imaging condition in seismic migration. *Geophysics*, **71**(6), S209–S217.

Weibull, W.W. and Arntsen, B. [2013] Automatic velocity analysis with reverse-time migration. *Geophysics*, **78**(4), S179–S192.